MINIMUM POWER INCREMENTAL CONTROL ALLOCATION USING REAL-TIME POWER MEASUREMENTS

Sinan Çimen Research Associate
Walter Fichter Professor
Institute of Flight Mechanics and Controls
University of Stuttgart
Stuttgart, Germany

ABSTRACT

This paper proposes a power-optimal incremental allocation scheme for over-actuated aircraft configurations. The proposed allocation scheme is built upon a baseline incremental nonlinear dynamic inversion (INDI) controller. The algorithm consists of a two-stage allocation scheme. First, the incremental pseudo controls are allocated in a direction-preserving manner when actuator saturation occurs. Second, a global objective function is minimized that provides global power optimality for the aircraft, by utilizing a null space transition scheme. Existing methods either minimize only L^1/L^2 norm of the actuator command increments, or use a power consumption model to construct a secondary objective function for the allocation. In this paper, we propose a secondary objective function that is dependent on the real-time power consumption of the actuators. The method does not require an energy model for the actuators, which can be cumbersome to approximate accurately. Nonlinear simulation results with a transition aircraft demonstrate reduced power consumption in comparison to existing model-based approaches.

INTRODUCTION

Over-actuated aircraft configurations have gained a great amount of popularity in the recent years. In particular, recent vertical take-off-and-landing (VTOL) aircraft concepts feature highly over-actuated propulsion systems, since electric propulsion is becoming increasingly cost-effective and efficient. Also, for manned operations, over-actuated systems provide safety in cases of actuator failures. As the number of these concepts grows, the control allocation problem, which deals with the distribution of the demanded forces and moments from the controller within the actuators of the aircraft, is becoming more important. There are several well-known methods implemented to solve the unconstrained control allocation problem, such as pseudoinverse-based methods and direct allocation methods (Ref. 1). Some pseudoinverse-based methods like Moore-Penrose pseudoinverse do not consider effector saturations. Meanwhile, daisy-chaining (Ref. 2) and Cascaded Generalized Pseudoinverse (CGI) methods (Refs. 3, 4) are able to handle effector saturations. Also, if the problem is formulated as an optimization problem, several approaches from the optimization literature can be used to solve the allocation problem, such as interior-point methods (Ref. 5) or active-set methods (Ref. 6). In applications where the allocation methods are used online, daisy-chaining and CGI-based methods are favorable because of their bounded run-time. In the case of unattainable moments, allocation methods can show either axis prioritization (Ref. 7) or direction-preserving behavior (Ref. 3). While axis prioritization methods assign higher priority to specific axes based on the mission definition, direction preserving methods scale the solution to the boundary of the polytope of attainable moments. Another aspect is that control allocation methods can be employed either as total command allocation schemes or as frame-wise or incremental allocation schemes (Ref. 8). The incremental allocation is inherently able to handle rate limits of the actuators. Also, it is able to handle effector nonlinearities due to the local computation of control effectiveness matrix. However, incremental allocation methods suffer from path-dependency, a phenomenon that causes aircraft to converge to different trim conditions based on the history of the state. Secondary objective functions are especially useful for optimizing a global objective function to solve path-dependency problem. In Ref. 9, an allocation scheme with secondary objective functions based on the expected intuitive behavior of the aircraft is proposed to address path-dependency issue. In Ref. 10, a minimum power secondary objective function is proposed to optimize power consumption of the aircraft, at the same time solving path-dependency problem.

Although any type of controller can be used with incremental allocation scheme, the baseline incremental nonlinear dynamic inversion (INDI) controller is inherently suitable. INDI is a sensor-based control approach, which outputs incremental pseudo controls to the allocation. Then, the incremental allocation method computes effector command increments. The incremental pseudo control vector represents increments in linear and angular accelerations. INDI control approach has been utilized for rate control for fixed-wing aircraft configurations (Refs. 6,11), as well as, for velocity control for transition VTOL aircraft configurations (Ref. 12), which gained popularity in recent years, because of their operability over a wide flight envelope. INDI mainly relies on sensor feedback for linear and angular accelerations, and is therefore robust against model uncertainties.

In this paper, a minimum power, incremental allocation method is proposed. The proposed method is a two-stage allocation scheme. First, the pseudo controls from the controller are allocated using a direction-preserving variant of CGI (Ref. 3). Then, a secondary allocation phase is employed, which acts on the null space of the control effectiveness matrix. This way, resulting forces and moments remain unchanged in the second phase. The secondary allocation phase optimizes the power consumption of the aircraft using the real-time power consumption feedback from effectors. This approach provides an optimization process for total effector commands, although both phases are acting in an incremental manner. The proposed method is employed with a baseline INDI controller with velocity, attitude, and angular rate loops. The algorithm is tested in simulation on a transition aircraft, which has eight fixed-tilt rotors in an asymmetric layout along the lateral axis. The allocation algorithm also computes optimal roll and pitch increments, which are fed back to the attitude loop, which results in optimized distribution of aerodynamic lift and propeller thrust for high velocity flight.

PRELIMINARIES

Incremental Nonlinear Dynamic Inversion

The following derivation is made with the assumption of relative degree of the system being one, which means that the first derivative of the output dynamics contains direct terms with the input. The general nonlinear aircraft dynamics expressed in the input non-affine form are given by:

$$\dot{x} = f(x(t), u(t)) \tag{1}$$

$$y = h(x(t)) \tag{2}$$

where $x \in \mathbb{R}^n$ is the state vector, $u \in \mathbb{R}^p$ the control input vector, and $y \in \mathbb{R}^m$ the output vector. Note that it is assumed that all states x are directly measurable. $f : \mathbb{D}_{x,u} \to \mathbb{R}^n$ is a nonlinear function depending on the state x and inputs u.

The nonlinear dynamics described in Eq. (1) and (2) can be controlled by either nonlinear dynamic inversion (NDI) or its incremental form INDI. INDI controller computes a pseudo control increment by linearizing the system at the current state and input, based on a Taylor series expansion. The state derivative can be written as:

$$\dot{x} \approx \dot{x}_0 + \frac{\partial f(x,u)}{\partial x}\bigg|_{x_0,u_0}(x - x_0) + \frac{\partial f(x,u)}{\partial u}\bigg|_{x_0,u_0}(u - u_0) + \text{h.o.t.} \tag{3}$$

where the variables $x_0, \dot{x}_0$, and u_0 with subscript 0 represent the values measured at the current time-step. Neglecting the terms higher than first order, Eq. (3) is expressed as:

$$\dot{x} \approx \dot{x}_0 + \frac{\partial f(x,u)}{\partial x}\bigg|_{x_0,u_0}(x - x_0) + \frac{\partial f(x,u)}{\partial u}\bigg|_{x_0,u_0}(u - u_0) \tag{4}$$

A core assumption of INDI-based flight control laws is the time scale separation assumption (Refs. 13,14). It is assumed that, if actuators in the system are fast enough, then they are dominant in the state derivative. In other words, if the actuator dynamics are significantly faster than the system dynamics, the term related to the state vector in the state derivative stated in Eq. (4) can be neglected. Another condition for time scale separation assumption is that sampling rate should be high enough. Based on the time scale separation assumption, Eq. (4) is simplified as:

$$\dot{x} = \dot{x}_0 + \frac{\partial f(x,u)}{\partial u}\bigg|_{x_0,u_0}(u - u_0) \tag{5}$$

The output dynamics given in Eq. (2) is derived once, which gives a relation between the output and the input:

$$\dot{y} \approx \dot{y}_0 + \frac{\partial h(x)}{\partial x}\bigg|_{x_0} \frac{\partial f(x,u)}{\partial u}\bigg|_{x_0,u_0}(u - u_0) \tag{6}$$

Substituting $B(x_0, u_0)$ to represent the partial differential part and defining input increment $\Delta u = u - u_0$, then Eq. (6) becomes:

$$\dot{y} \approx \dot{y}_0 + B(x_0, u_0)\Delta u \tag{7}$$

Finally, the control input u is derived as

$$u = u_0 + B^+(x_0, u_0)(\nu - \dot{y}_0) \tag{8}$$

where the pseudo controls ν is defined by $\nu = \dot{y}_{\text{des}}$. B^+ denotes the pseudoinverse of B. In the case of square B matrix ($n = p$), the inverse of B is used directly. Another assumption for INDI is that $x_0, \dot{y}_0$ and u_0 are measurable or can be approximated (Ref. 15). The desired trajectory $\dot{y}_{\text{des}}$ can be designed using a linear control law K and the error in the outer loop e, such that $\dot{y}_{\text{des}} = Ke$. For the systems having a relative degree higher than one, the inner-most controller can be designed using the derivation above, and outer-loop controllers can be designed with any preferred controller design method by cascading. The overall control system design in this work is described later in this section.

Global Control Allocation

Generally, control allocation problem is handled in a way that the absolute commands to actuators are calculated in each time-step. Therefore, inputs to the allocation are absolute force and moment commands. The relationship between actuator inputs and the resulting pseudo controls is typically expressed as:

$$Bu = \boldsymbol{\nu} \tag{9}$$

where $B \in \mathbb{R}^{m \times p}$ is the control effectiveness matrix that maps the actuator inputs to pseudo controls, $u \in \mathbb{R}^p$ is the actuator command vector and $\boldsymbol{\nu} \in \mathbb{R}^m$ is the desired pseudo control vector. For a 6-DOF allocation scheme, $m = 6$, consisting of three forces and three moments.

For an exactly determined system, where $m = p$, the solution is given by the direct inverse:

$$u = B^{-1}\boldsymbol{\nu} \tag{10}$$

In most aerospace applications, the systems are over-actuated ($p > m$). In such cases, an exact inverse does not exist, and a pseudoinverse-based method is a possible solution. The weighted Moore-Penrose pseudoinverse provides a least-squares solution while incorporating a weighting matrix W to prioritize axes in pseudo controls. The weighted pseudoinverse of the control effectiveness matrix, denoted as B_W^+, is computed as follows:

$$B_W^+ = (B^T W B)^{-1} B^T W \tag{11}$$

where $W \in \mathbb{R}^{n \times n}$ is a positive definite weighting matrix that assigns priority to different axes of pseudo controls.

The optimal actuator command is then determined using:

$$u = B_W^+ \boldsymbol{\nu} \tag{12}$$

In the case of actuator saturations and rate limits, following conditions are needed to be satisfied by the allocation algorithm:

$$\underline{u}_i < u_i < \overline{u}_i \tag{13}$$

$$\underline{u}_i = max(u_{i,\min}, u_{i,0} - \tau_s \dot{u}_{i,\min}) \tag{14}$$

$$\overline{u}_i = min(u_{i,\max}, u_{i,0} + \tau_s \dot{u}_{i,\max}) \tag{15}$$

where $u_{i,\min}$ and $u_{i,\max}$ are positional limits. $\dot{u}_{i,\min}$ and $\dot{u}_{i,\max}$ are rate limits. $u_{i,0}$ is the estimated or measured actuator state.

Incremental Control Allocation

When INDI is used as baseline control strategy, the allocation problem takes the incremental form as:

$$B\Delta u = \Delta\boldsymbol{\nu} \tag{16}$$

where, in this case, B matrix is evaluated locally with the current state and actuator positions. The same approach presented for global control allocation can also be utilized for this problem. However, the weighted Moore-Penrose algorithm only minimizes a weighted L^2-norm of the incremental command for such problem. This leads to the path-dependency problem, where resulting actuator commands can be different for cases with the same system states, depending on the past trajectory of the system.

To address path-dependency issue, a secondary objective function that optimizes global properties of the system can be implemented. To compute the additional increment, null space of the local control effectiveness matrix B, $\mathcal{N}(B)$, is used. This way, the actuator commands are driven towards a favorable configuration, while keeping the resulting pseudo controls the same. This additional objective function can be constructed using a power consumption model (Ref. 16), so that actuators are moved towards an energy-optimal configuration. Then, the additional increment is summed with the nominal increment calculated in the first allocation step, such that:

$$\Delta u_{\text{cmd}} = \Delta u_{\text{nom}} + K^* \Delta u^{\perp} \tag{17}$$

where $\Delta u^{\perp}$ is the direction of the additional increment, Δu_{nom} is the nominal increment. K^* is the optimal scaling factor, which is described in a later section in detail.

Control System Architecture

The implemented control architecture is an incremental control and allocation scheme, similar to Ref. 17. The architecture is depicted in Fig. 1. The remote pilot commands x, y and z velocities in the control frame, denoted by c, which is a local geodetic frame rotated by aircraft's yaw angle. The yaw rate is also commanded by the pilot. The architecture includes a cascaded control structure for velocity, attitude and attitude rate, all of them being linear control laws. The pseudo controls from controllers to the allocation are:

$$\boldsymbol{\nu} = \begin{bmatrix} {}_c\dot{v}_x & {}_c\dot{v}_y & {}_c\dot{v}_z & \dot{p} & \dot{q} & \dot{r} \end{bmatrix}^T \tag{18}$$

Angular accelerations are obtained by deriving angular rate measurements from the gyroscope. Then, they are filtered with a low-pass filter with a corner frequency of $\omega_{\ddot{\Psi}}$. Bandwidth of the each loop in cascade is separated by a factor of k. That is, bandwidth for the attitude rate controller is $\omega_{\dot{\Psi}} = \omega_{\ddot{\Psi}}/k$, and for the attitude controller, it is $\omega_{\Psi} = \omega_{\dot{\Psi}}/k$. Similarly, bandwidth of the velocity controller is $\omega_v = \omega_{\Psi}/k$. The pilot commands are filtered with a reference model as shown in Fig. 1. In this work, second-order filters are used as reference models.

Pitch and roll increments are also included in the allocation as virtual effectors, which are fed back to the attitude controller. Partial derivatives of pseudo controls with respect to attitude increments are also included in the control effectiveness ma-

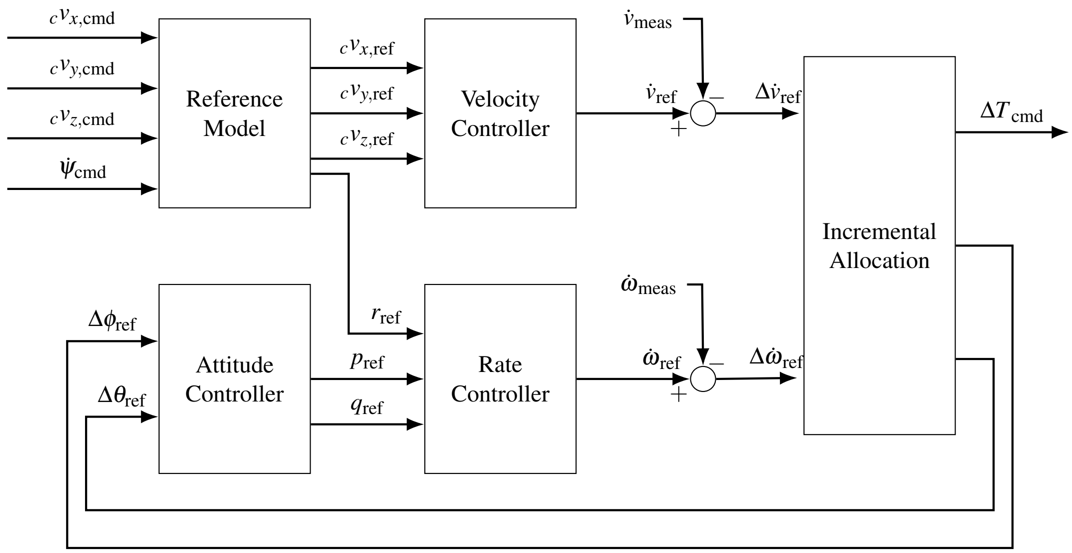

Figure 1. INDI control system architecture.

trix as:

$$B = \begin{bmatrix} \frac{\partial {}_c\dot v_x}{\partial T_1} & \frac{\partial {}_c\dot v_x}{\partial T_2} & \dots & \frac{\partial {}_c\dot v_x}{\partial \phi} & \frac{\partial {}_c\dot v_x}{\partial \theta} \\ \frac{\partial {}_c\dot v_y}{\partial T_1} & \frac{\partial {}_c\dot v_y}{\partial T_2} & \dots & \frac{\partial {}_c\dot v_y}{\partial \phi} & \frac{\partial {}_c\dot v_y}{\partial \theta} \\ \frac{\partial {}_c\dot v_z}{\partial T_1} & \frac{\partial {}_c\dot v_z}{\partial T_2} & \dots & \frac{\partial {}_c\dot v_z}{\partial \phi} & \frac{\partial {}_c\dot v_z}{\partial \theta} \\ \frac{\partial \dot p}{\partial T_1} & \frac{\partial \dot p}{\partial T_2} & \dots & 0 & 0 \\ \frac{\partial \dot q}{\partial T_1} & \frac{\partial \dot q}{\partial T_2} & \dots & 0 & 0 \\ \frac{\partial \dot r}{\partial T_1} & \frac{\partial \dot r}{\partial T_2} & \dots & 0 & 0 \end{bmatrix} \tag{19}$$

The output of the allocation are thrust commands for each motor. Then, these thrust commands are mapped into PWM commands using the empirical data of the motors.

MINIMUM POWER INCREMENTAL CONTROL ALLOCATION

This section represents how to compute the additional increment, so that the resulting commands of the allocation method are driven towards the power optimal configuration. The additional increment $\Delta u^{\perp} \in \mathcal{N}(B)$ computed with a second allocation scheme that extends both the local control effectiveness matrix and incremental pseudo controls, B as B^* and $\Delta\boldsymbol{\nu}$ as $\Delta\boldsymbol{\nu}^*$ (Ref. 16). An objective function for power consumption is defined as:

$$J = f(\Delta u_{\text{cmd}}, u_0) \tag{20}$$

The function f is described in this section and in the Appendix for measured power and model-based power cases, respectively. The partial derivative of this objective function with respect to incremental actuator commands is added as a row to the control effectiveness matrix as:

$$B^* = \begin{bmatrix} & B & \\ \frac{\partial J_1}{\partial \Delta u_1} & \frac{\partial J_2}{\partial \Delta u_2} & \dots \end{bmatrix} \tag{21}$$

Then, the pseudo control vector is also extended by a row, which should be an arbitrary negative number for the result to be in power reducing direction. Other rows are of the pseudo controls are zero, so that resulting forces and moments do not change.

$$\Delta\boldsymbol{\nu}^* = \begin{Bmatrix} \mathbf{0} \\ a \end{Bmatrix}, \quad a < 0 \tag{22}$$

$$\Delta u^{\perp} = B^{*+}\Delta\boldsymbol{\nu}^* \tag{23}$$

Power Optimization using Power Measurements

The method given in the Appendix relies on a propeller model, which is not easy to obtain and can significantly deviate from real required power because of many reasons, such as wear of the propeller surface, elasticity effects, propeller-airframe or propeller-ground interactions, and heating of the motors. Therefore, using sensor feedback to calculate the power constants for each motor provides a more accurate power consumption objective function. In this section, the secondary objective function based on online power consumption measurements is presented. Since the output of the allocation is the thrust created by the corresponding propeller, the power consumption must be expressed in terms of the thrust T. Generally, the required power and propeller thrust has the relation (Ref. 18):

$$P \propto T^{3/2} \tag{24}$$

The power consumption of electric motors is usually available in ESCs through voltage and current measurements. It can also be measured using external sensors. Denote $\tilde{P}_i$ as the measured power consumption of the actuator i. Then, using the relation given in Eq. (24), a power coefficient for i-th actuator can be calculated as:

$$c_{p,i} = \frac{\tilde{P}_i}{T_{0,i}^{3/2}} \tag{25}$$

where $T_{0,i}$ is the estimated or measured thrust of the i-th propeller. In simulations presented in this paper, the current thrust of the propeller is estimated by filtering commanded thrusts with a first-order filter, with time constant computed from empirical data.

Then, the power optimality objective function and its partial derivative with respect to propeller thrust can be defined as:

$$J_i = c_{p,i} T_i^{3/2} \tag{26}$$

$$\frac{\partial J_i}{\partial \Delta T_i} = \frac{3}{2} c_{p,i} T_i^{1/2} \tag{27}$$

Note that, in the row corresponding to the partial derivative of required power, only the elements corresponding to propellers are nonzero. Other elements corresponding to attitude increments are zero since they do not have direct effect on power consumption. However, through decreasing total power demand of the propellers, the attitude increments are also driven towards the power optimal values. The extended control effectiveness matrix for power optimality through measurements can be constructed as:

$$B^* = \begin{bmatrix} & B & \\ \frac{3}{2} c_{p,1} T_1^{1/2} & \frac{3}{2} c_{p,2} T_2^{1/2} & \dots \end{bmatrix} \tag{28}$$

With the extended control effectiveness matrix given in Eq. (28) and the extended pseudo controls given in Eq. (22), the direction of the additional increment can be calculated with a pseudoinverse method, as in Eq. (23). Note that $\Delta u^{\perp}$ provides only the direction towards minimum-power configuration, since a is arbitrary. It should be scaled to find the true optimal increment and not to exceed actuator limits. The derivation of the scaling factor is given in the next section.

Optimal Scaling Factor

An optimal scaling factor needs to be found, since $\Delta u^{\perp}$ only gives the direction of the command increment towards power-optimal configuration. The length of the vector needs to be adjusted using the scale factor. The value of K^* can be found by calculating the root of $\frac{\partial J}{\partial K}$, with an approach similar to (Ref. 16). $\frac{\partial J}{\partial K}$ can be separated as:

$$\frac{\partial J}{\partial K} = \frac{\partial J}{\partial u} \frac{\partial u}{\partial K} = 0 \tag{29}$$

Substituting Eq. (37) (or Eq. (27) for measured power case) and differentiating Eq. (17), Eq. (29) becomes:

$$\left(\frac{3}{2} \mathbf{C} u^{1/2}\right) \Delta u^{\perp} = \left(\frac{3}{2} \mathbf{C} (u_0 + \Delta u_{\text{nom}} + K^* \Delta u^{\perp})^{1/2}\right) \Delta u^{\perp} = 0 \tag{30}$$

Note that $\mathbf{C}$ is the vector of coefficients either c_i or $c_{p,i}$ for model-based or measured power optimality cases, respectively. u is the vector of total commands of the actuators and u_0 is the vector of actuator commands in the previous timestep.

Using B^* from Eq. (28) and substituting into Eq. (23) to calculate a as:

$$a = \frac{3}{2} \mathbf{C} (u_0 + \Delta u_{\text{nom}}) \Delta u^{\perp} \tag{31}$$

Then, using a to simplify Eq. (30):

$$\frac{3}{2} \mathbf{C} K^{*1/2} (\Delta u^{\perp})^{3/2} = -a \tag{32}$$

Rearranging to calculate K^* as:

$$K^* = \left(\frac{-a}{3 \mathbf{C} (\Delta u^{\perp})^{3/2}} \right)^2 \tag{33}$$

Note that, although the optimal scale factor is computed, the total command increment may exceed actuator saturation limits and rate limits. Therefore, a direction-preserving scaling of the resulting incremental command is applied, such that only one actuator is saturated by the resultant command. A similar scaling factor is calculated in (Ref. 3).

SIMULATION RESULTS ON A TRANSITION AIRCRAFT

Aircraft Setup

The configuration used in the simulations is given in Fig. 2. The propellers of the aircraft are identical and symmetric along the x-axis of the aircraft. Each propeller has different fixed-tilt angle, and the tilt angles of propellers 1-6 are relatively small, so that they mainly produce vertical thrusts. The rear propellers are tilted 30° in pitch, which means that they produce a mixture of vertical and horizontal thrust. The electric motors are modeled through first-order transfer functions, with a time constant computed from experimental data. Aerodynamic coefficients are obtained from wind tunnel tests of the aircraft. The mapping from propeller thrust to PWM commands is derived from experimental data from real propellers. The simulation update rate is set to 200 Hz.

The implemented INDI baseline controller provides a unified control approach for all flight phases of the aircraft. At low velocities, the vehicle operates mainly with propeller thrusts. During transition, vehicle gradually unloads propeller commands and starts to utilize aerodynamic lift. Since the vehicle has no aerodynamic control surfaces, and propellers are not shut off during any flight phase, maneuvers at high velocities are carried out by the propellers.

Results

This section presents simulation results for both the proposed allocation method with power measurements presented in the previous section, and allocation with model-based power optimization presented in the Appendix. It is assumed that some

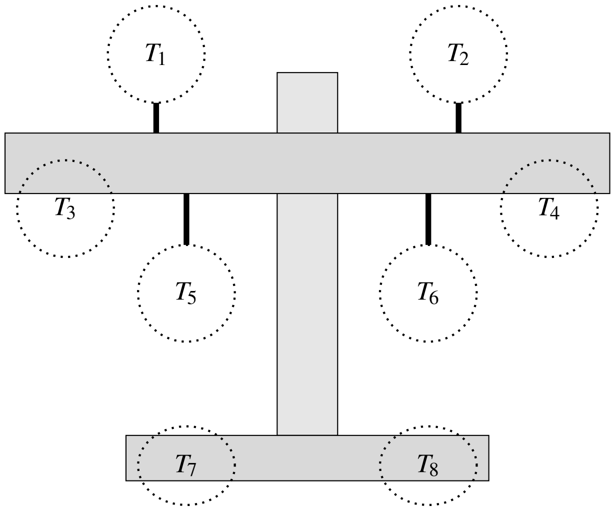

Figure 2. Vehicle configuration.

of the propellers are degraded with a loss factor $\lambda_{i,\text{loss}}$, such that $P_{i,\text{actual}} = \lambda_{i,\text{loss}} P_{i,\text{nom}}$, where $P_{i,\text{nom}}$ is the expected power consumption of i-th propeller based on the model described in the Appendix.

A maneuver from hover to high speed flight, where a mixture of aerodynamic lift and propeller thrust is present on the aircraft, is simulated. In the simulations, propellers 3 and 4 are assumed to be degraded by the same factor $\lambda_{3,\text{loss}} = \lambda_{4,\text{loss}} = 1.25$. For other propellers, the loss factor is assumed to be one(no degradation). The commanded and actual velocity in the x axis of the c frame are given in Fig. 3. Angle of attack during the maneuver is given in Fig. 4. Since a pure horizontal flight is presented, angle of attack and pitch angle are assumed to be equal $\alpha \approx \theta$. The vehicle hovers at $\alpha \approx 8^\circ$ and it pitches down to $\alpha \approx -4^\circ$ during transition. During the constant high-speed flight, the vehicle maintains an angle of attack $\alpha \approx 1^\circ$, and when transitioning from high speed flight to hover flight, it reaches an angle of attack of $\alpha \approx 12^\circ$.

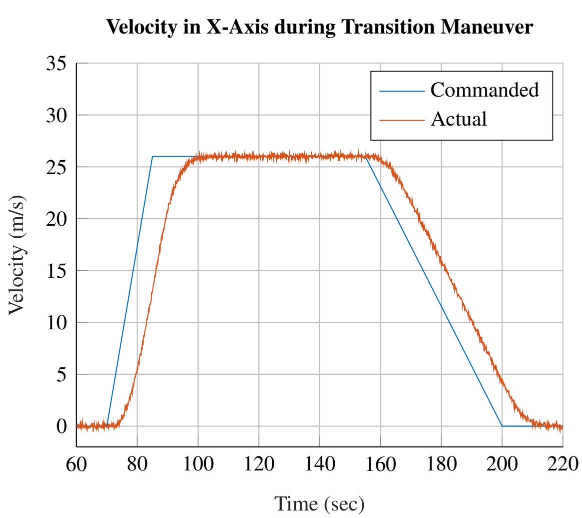

Figure 3. Commanded vs actual velocity in x-axis of c frame.

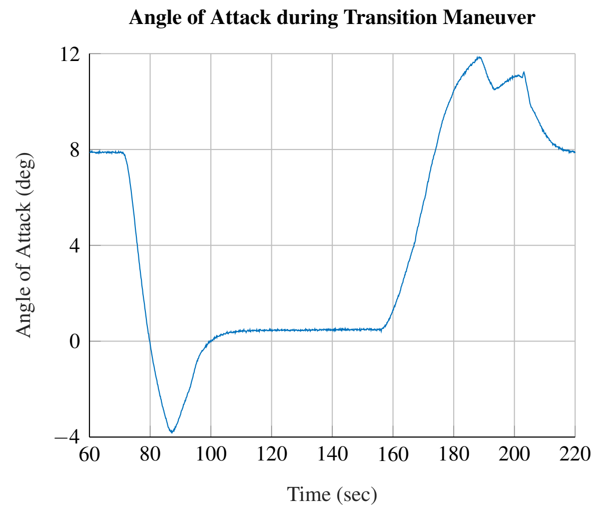

Figure 4. Angle of attack of the aircraft during transition.

Since the simulated maneuver includes only a command along the x axis, thrusts of counter propellers along x axis are nearly identical, which are propeller pairs 1-2, 3-4, 5-6 and 7-8. For the sake of visibility, only one thrust from each pair is drawn in the following figures. In Fig. 5, thrust commands of each propeller are given for the model-based power optimization case. In Fig. 6, thrust commands are given for the measured power optimization case. During transition and high speed flight phases, rear propellers speed up since they are the main forward force source. Similarly, while slowing down, the thrusts of the rear motors decrease, and the first six propellers apply more thrust to create a positive moment along the y-axis. When the outputs of model-based and measurement-based optimization methods are compared, it can be seen that measurement-based algorithm outputs less thrust with respect to model-based algorithm for propellers 3 and 4; since their efficiencies are lower than other propellers.

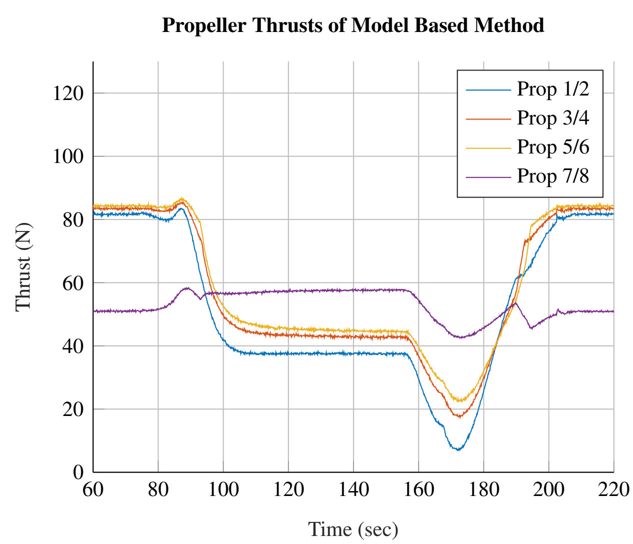

Figure 5. Thrusts of each propeller pair, resulting from model-based power optimization.

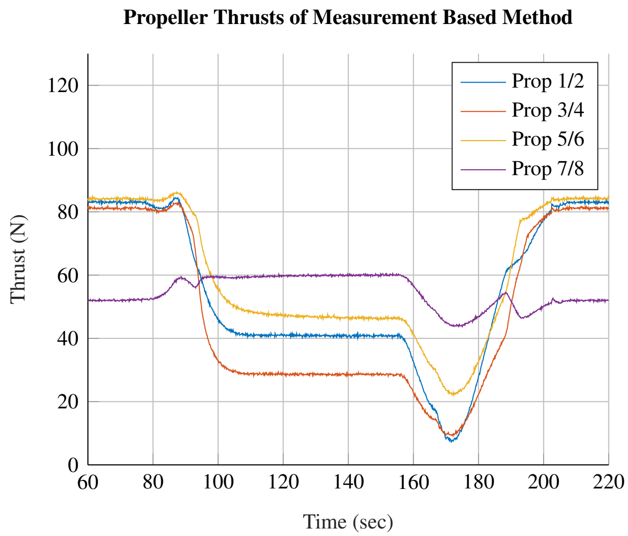

Figure 6. Thrusts of each propeller pair, resulting from measurement-based power optimization.

In Fig. 7, the power consumptions of the two simulated cases are drawn. The power consumption first increases at the start of the transition maneuvers, then it decreases sharply with increasing airspeed. Although the difference between power consumption resulting from model-based and measurement-based objective functions is small at hover and low-speed flight, it becomes significant at higher speed flight. In the high-speed flight regime, the proposed method requires $\sim$8% lower power than the model-based approach. The difference between two methods would be higher with an higher deviation of power consumption of motors from their modeled consumption.

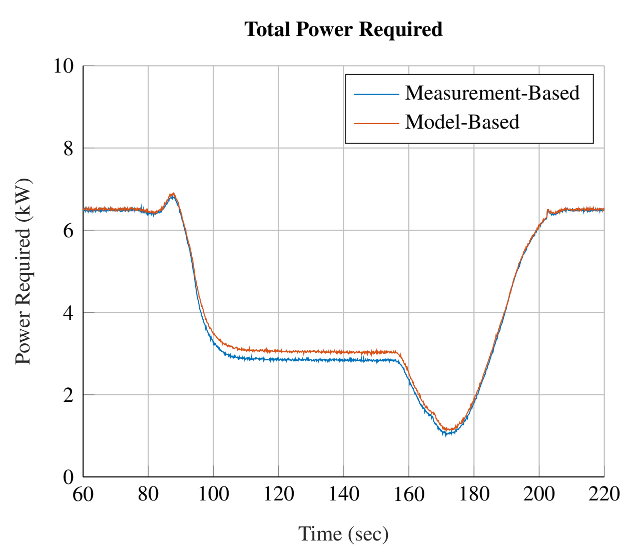

Figure 7. Required power for measurement-based and model-based optimization methods during allocation.

CONCLUSIONS

This paper proposed an incremental allocation scheme which optimizes power consumption based on real-time power measurements of motors of an over-actuated aircraft. To achieve that, a two-staged allocation is employed. In the first stage, required forces and moments are allocated to the actuator commands. In the second stage, the solution is moved in the null space of the control allocation matrix, so that the power optimality objective function, which is constructed using power measurements, is minimized. Utilizing power consumption in the objective function eliminates the modeling need of propellers' power consumption, which can be cumbersome. Also, several unmodeled effects on the power consumption of the propeller like mechanical wear and elasticity can be addressed with this approach. The proposed method is compared with an allocation scheme, where the power optimality objective function is constructed using a power consumption model. Nonlinear simulations of a transition vehicle, whose velocity is controlled using INDI controller, are conducted. Some propellers are assumed to have degradation, so that a deviation from the power consumption model is present. Results show that utilizing power measurements decreases the overall power consumption significantly, especially at high airspeeds. Effect of using power measurements on overall power consumption can be analyzed for different transition aircraft configurations. The effectiveness of the proposed method is to be demonstrated in a flight test in future.

Author contact:
Sinan Çimen: sinan.cimen@ifr.uni-stuttgart.de
Walter Fichter: fichter@ifr.uni-stuttgart.de

APPENDIX: MODEL-BASED POWER OPTIMIZATION

In this section, the derivation of the power optimality objective, that is used for comparison with the proposed approach in the results, is given. An objective function based on a simplified model for power consumption of each propeller with respect to the propeller thrust, which is independent of any sensor feedback, is derived. The required power for a propeller at a given rotational speed is (Ref. 18):

$$P = c_p \rho n^3 d^5 \tag{34}$$

where c_p is the power coefficient, ρ is the air density, n is the rotational speed of the propeller and d is the propeller diameter. Substituting $c_p = 2\pi c_q$, where c_q is the torque coefficient of the propeller, to Eq. (34):

$$P = 2\pi c_q \rho n^3 d^5 \tag{35}$$

Substituting the relation between propeller speed and the thrust $n = \sqrt{\frac{T}{c_T \rho d^4}}$, where c_T is the thrust coefficient, Eq. (35) becomes:

$$P = 2\pi c_q \rho \left(\frac{T}{c_T \rho d^4}\right)^{3/2} d^5 = 2\pi c_q \rho^{-1/2} c_T^{-3/2} T^{3/2} d^{-1} \tag{36}$$

The partial derivative of the required power with respect to thrust is:

$$\frac{\partial P}{\partial T} = 3\pi c_q \rho^{-1/2} c_T^{-3/2} d^{-1} T^{1/2} \triangleq \frac{3}{2} c T^{1/2} \qquad (37)$$

where $c \triangleq 2\pi c_q \rho^{-1/2} c_T^{-3/2} d^{-1}$. Then, the extended control effectiveness matrix B^* can be computed by adding a row, which consists of corresponding partial derivatives of the required power for each actuator, as:

$$B^* = \begin{bmatrix} & B & \\ \frac{3}{2}c_1 T_1^{1/2} & \frac{3}{2}c_2 T_2^{1/2} & \dots \end{bmatrix} \qquad (38)$$

With the extended control effectiveness matrix given in Eq. (38) and an extended pseudo controls vector—whose rows corresponding to moments and forces are zeros to keep the resulting forces and moments the same as the result of the first stage of the allocation, as given in Eq. (22)—the direction of the additional increment is calculated using a pseudoinverse. The magnitude of the increment in that direction is again calculated with the same method presented in Optimal Scaling Factor section. Similarly, the increment is scaled in the case of actuator saturations, so that the total command conforms actuator limits and only one actuator command is on the boundary of the actuator position limits, similar to the scaling applied in (Ref. 3).

ACKNOWLEDGMENTS

This work is supported by the Bavarian Ministry of Economic Affairs, Regional Development and Energy, through the research program H-AMI 2 in the project AMI-PGS.

REFERENCES

1. Durham, W. C., "Constrained control allocation," *Journal of Guidance, Control, and Dynamics*, Vol. 16, (4), 1993, pp. 717–725. DOI: 10.2514/3.21072.

2. Oppenheimer, M. W., Doman, D. B., and Bolender, M. A., "Control Allocation for Over-actuated Systems," 2006 14th Mediterranean Conference on Control and Automation, 7 2006. DOI: 10.1109/MED.2006.328750.

3. Stephan, J., and Fichter, W., "Fast Exact Redistributed Pseudoinverse Method for Linear Actuation Systems," *IEEE Transactions on Control Systems Technology*, Vol. 27, (1), 2019, pp. 451–458. DOI: 10.1109/TCST.2017.2765622.

4. Jin, J., "Modified Pseudoinverse Redistribution Methods for Redundant Controls Allocation," *Journal of Guidance, Control, and Dynamics*, Vol. 28, (5), 2005, pp. 1076–1079. DOI: 10.2514/1.14992.

5. Petersen, J., and Bodson, M., "Interior-Point Algorithms for Control Allocation," *Journal of Guidance Control and Dynamics*, Vol. 28, 05 2005, pp. 471–480. DOI: 10.2514/1.5937.

6. Heer, P., De Visser, C., Hoogendoorn, M., and Jentink, H., "Incremental Nonlinear Control Allocation for an Aircraft with Distributed Electric Propulsion," AIAA SCITECH 2023 Forum, 01 2023. DOI: 10.2514/6.2023-1248.

7. Pfeifle, O., and Fichter, W., "Incremental Control Allocation with Axis Prioritization on the Boundary of the Attainable Control Set," AIAA SCITECH 2023 Forum, 01 2023. DOI: 10.2514/6.2023-1639.

8. Durham, W., Bordignon, K. A., and Beck, R., *Frame-wise Control Allocation*, John Wiley & Sons, Ltd, 2016, Chapter 7, pp. 139–160. DOI: https://doi.org/10.1002/9781118827789.ch7.

9. Zhang, J., Bhardwaj, P., Raab, S., Saboo, S., and Holzapfel, F., "Control Allocation Framework for a Tiltrotor Vertical Take-off and Landing Transition Aircraft Configuration," 2018 Applied Aerodynamics Conference, 06 2018. DOI: 10.2514/6.2018-3480.

10. Pfeifle, O., and Fichter, W., "Minimum Power Control Allocation for Incremental Control of Over-Actuated Transition Aircraft," *Journal of Guidance, Control, and Dynamics*, Vol. 46, 11 2022, pp. 286–300. DOI: 10.2514/1.G006929.

11. Stougie, J., Pollack, T., and Van Kampen, E.-J., "Incremental Nonlinear Dynamic Inversion control with Flight Envelope Protection for the Flying-V," AIAA SCITECH 2024 Forum, 01 2024. DOI: 10.2514/6.2024-2565.

12. Raab, S., Zhang, J., Bhardwaj, P., and Holzapfel, F., "Proposal of a Unified Control Strategy for Vertical Take-off and Landing Transition Aircraft Configurations," 2018 Applied Aerodynamics Conference, 06 2018. DOI: 10.2514/6.2018-3478.

13. Sieberling, S., Chu, Q. P., and Mulder, J. A., "Robust Flight Control Using Incremental Nonlinear Dynamic Inversion and Angular Acceleration Prediction," *Journal of Guidance, Control, and Dynamics*, Vol. 33, (6), 2010, pp. 1732–1742. DOI: 10.2514/1.49978.

14. Wang, X., van Kampen, E.-J., Chu, Q., and Lu, P., "Stability Analysis for Incremental Nonlinear Dynamic Inversion Control," *Journal of Guidance, Control, and Dynamics*, Vol. 42, (5), 2019, pp. 1116–1129. DOI: 10.2514/1.G003791.

15. van 't Veld, R., Van Kampen, E.-J., and Chu, Q., "Stability and Robustness Analysis and Improvements for Incremental Nonlinear Dynamic Inversion Control," 2018 AIAA Guidance, Navigation, and Control Conference, 01 2018. DOI: 10.2514/6.2018-1127.

16. Pfeifle, O., and Fichter, W., "Energy Optimal Control Allocation for INDI Controlled Transition Aircraft," AIAA Scitech 2021 Forum, 01 2021. DOI: 10.2514/6.2021-1457.

17. Pfeifle, O., *Incremental control and allocation for power-optimal flight of transition aircraft*, Dissertation, Universität Stuttgart, 2024.

18. Leishman, J. G., *Principles of Helicopter Aerodynamics*, Cambridge University Press, second edition, 2006, Chapter 2, pp. 55–115. DOI: 10.1017/S0001924000087352.